

## Counting errors in a voltage-biased electron pump

Xavier Jehl,\* Mark W. Keller, R. L. Kautz, J. Aumentado, and John M. Martinis  
*National Institute of Standards and Technology, 325 Broadway, Boulder, Colorado 80305*

(Received 2 December 2002; revised manuscript received 24 February 2003; published 30 April 2003)

We have measured the counting errors of a seven-junction electron pump when charge is pumped against a voltage difference. At finite bias voltages, we find that the errors increase exponentially with both pump voltage and temperature, in agreement with theoretical predictions. To compare experiment and simulation, all pump parameters were determined by independent electron-box experiments. Although we assume temperatures somewhat higher than those measured, simulations based on the ground-capacitance model yield excellent quantitative agreement with experiment and indicate that errors in the high-voltage regime are due to thermally activated tunneling. In addition, a surprising asymmetry between positive and negative voltages is explained by an asymmetry in the junction capacitances.

DOI: 10.1103/PhysRevB.67.165331

PACS number(s): 73.23.Hk, 85.35.Gv, 06.20.Fn

### I. INTRODUCTION

Since its introduction in 1991,<sup>1</sup> the electron pump has shown promise as a standard for both current<sup>1</sup> and capacitance,<sup>2</sup> applications recently reviewed by Keller.<sup>3</sup> In operation, the pump transfers charge from input to output, one electron at a time, through a series of small-area tunnel junctions and intervening metallic islands. The charge moves in response to bias voltages applied sequentially to the islands through gate capacitors, creating a traveling potential well that is able to store just one electron. The ultimate success of the pump in metrology is entirely dependent on transferring that one electron without significant chance of error. In the present paper, we explore the error rate of a pump used as a capacitance standard when charge transfer is opposed by a voltage difference between the input and output electrodes. We report both experiment and simulation. Our study is significant technologically because it sets a bound on the pump voltage required for accurate operation and scientifically because it explores pump errors in a new regime.

Error processes in the electron pump have previously been studied both experimentally<sup>1,4-11</sup> and theoretically.<sup>12-21</sup> In general, errors in the pump result either when an electron fails to tunnel as required or when it tunnels to an unwanted state. Failure-to-tunnel errors dominate at high operating speeds when insufficient time is allowed for the electron to tunnel to a lower energy state. Such errors have been observed experimentally in five- and seven-junction pumps by Martinis *et al.*<sup>4,5,10</sup>

Other errors, due to unwanted tunneling, require that the pump pass through an intermediate state of higher energy, either by cotunneling, thermally activated tunneling, or photon-assisted tunneling. In cotunneling, electrons tunnel in two or more junctions simultaneously, such that the high-energy intermediate state is virtual and the final state is lower in energy than the initial state. Errors due to cotunneling have been observed experimentally by Lotkhov *et al.*<sup>11</sup> in a three-junction pump. Cotunneling becomes less important in pumps with more junctions, and Kautz *et al.*<sup>9</sup> have shown that cotunneling does not explain the error rates observed in a seven-junction pump. Instead, under optimum bias conditions, errors in the seven-junction pump are dominated by

single-junction, photon-assisted tunneling.<sup>10</sup> In this case, the higher-energy intermediate state is reached with the help of a microwave photon apparently associated with the same noise source as the low-frequency  $1/f$  noise observed in single-electron-transistor (SET) electrometers. In the present study, we find that, with an applied voltage bias, errors in a seven-junction pump are dominated by thermally activated tunneling. Here, the bias voltage lowers the energy of the intermediate state, and thermal energy is sufficient to boost charges over the barrier and cause errors. With this result, all of the basic error mechanisms have now been observed in various pumps under various operating conditions: failure to tunnel, unwanted cotunneling, unwanted photon-assisted tunneling, and unwanted thermally activated tunneling.

The remainder of this paper is outlined as follows. In Sec. II, we describe the basic mechanism of the electron pump and present the equations that allow detailed simulation of its dynamics, including thermally activated tunneling, photon-assisted tunneling, and self-heating. In Sec. III, we describe the experimental procedures used to evaluate the circuit parameters of the pump and operate the pump as a capacitance standard. Finally, in Sec. IV, we compare the counting errors as determined by theory and experiment and describe the principal error mechanism active at finite bias voltages.

### II. THEORY

We consider the electron pump in the context of the ground-capacitance model,<sup>9,12</sup> using the equivalent circuit shown in Fig. 1. The pump is a series array of  $N$  small-area tunnel junctions with capacitances  $C_J$  and tunnel resistances  $R_J$ . Here,  $R_J$  and  $C_J$  are used to represent a generic junction,

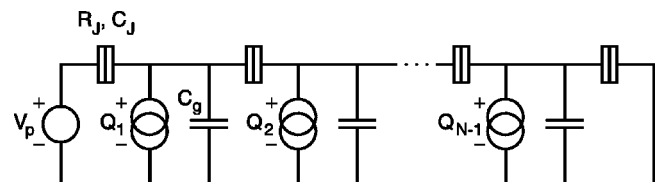


FIG. 1. Equivalent circuit of an  $N$ -junction electron pump within the ground-capacitance model. Nanoscale tunnel junctions are indicated by boxes.

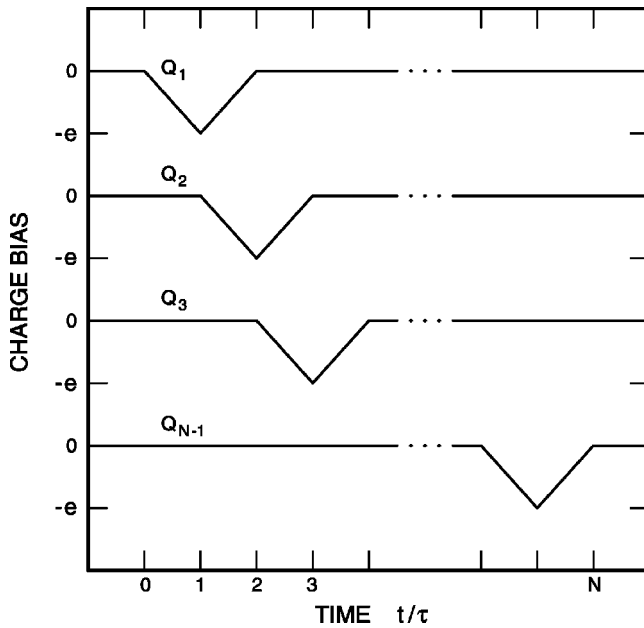


FIG. 2. Charge biases applied to the  $N-1$  gates of an  $N$ -junction pump to transfer a charge  $e$  through the pump.

without precluding the possibility of differences between junctions. The  $N-1$  intervening islands have capacitances  $C_g$  to ground and are biased by charge sources  $Q_1$  through  $Q_{N-1}$ . The pump is generally connected to an external capacitance that is much larger than  $C_J$  or  $C_g$ , and in Fig. 1 we represent this capacitance by the voltage source  $V_p$ . Ideally, the pump is operated with  $V_p=0$ , but in the present study we consider the effect of a nonzero bias voltage.

To transfer an electron from input to output, the pump is biased by triangular charge pulses applied sequentially to each of the  $N-1$  islands, as shown in Fig. 2. Each pulse is of amplitude  $-e$  and duration  $2\tau$ . Because the pulses overlap, the bias cycle is completed in a time of  $N\tau$ , transferring a charge through all  $N$  junctions of the pump. Reversing the order of the pulses pumps a charge in the opposite direction.

The operation of the pump is most easily understood in terms of electrostatic energy. In Fig. 3, we show the energy of a seven-junction pump at a series of times throughout the pump cycle. At each time, a solid line plots the energy as a function of the location of an extra charge among the six islands. Here, island numbers 0 and 7 denote the input and output electrodes. At  $t/\tau=0$  and 0.5, the energy of the pump would be raised if an extra charge were added to any island, and this ‘‘Coulomb blockade’’ prevents a charge from entering the pump. However, with a full bias charge of  $-e$  applied to the first island at  $t/\tau=1$ , an energy well is created and a charge can tunnel onto island 1. In Fig. 3, a dot indicates the minimum-energy location of the added charge and shows its progress through the pump. In each plot, a dashed line shows the energy of the pump if a second extra charge were added to one of the islands, assuming that the first charge is at the energy minimum. Thus at  $t/\tau=1$  a second charge is prevented from tunneling onto island 1 by this energy barrier. As charge biases are applied to successive islands of the pump, the energy well moves from island to

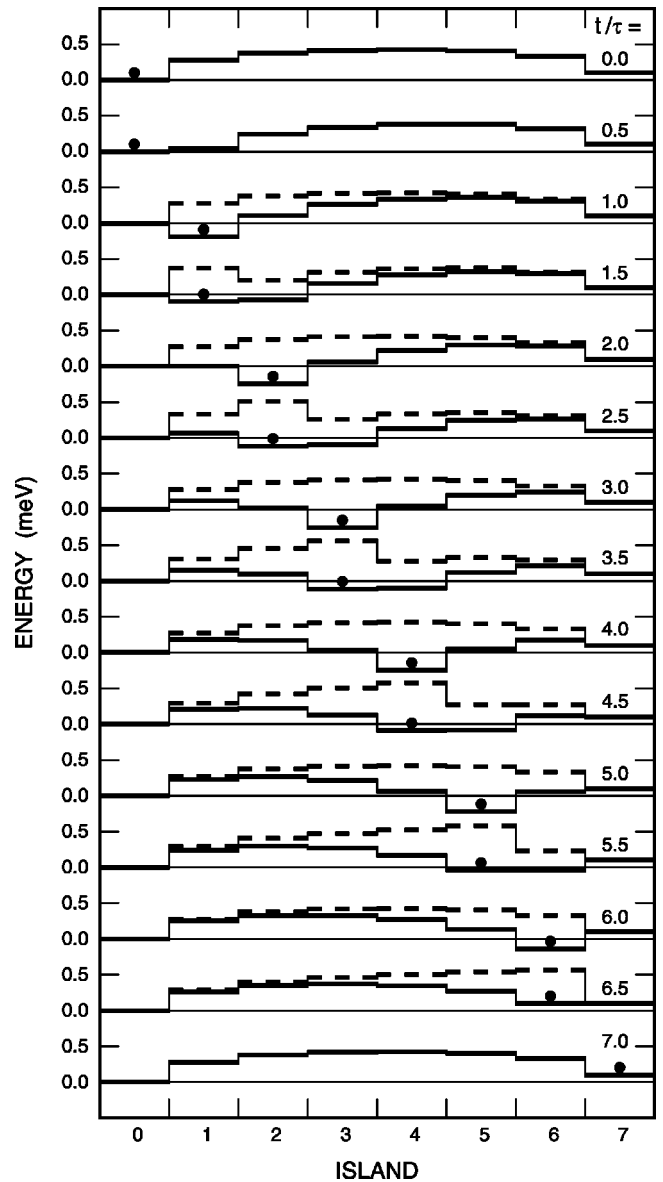


FIG. 3. Electrostatic energy of a seven-junction pump with a bias voltage  $V_p = -0.1$  mV at a series of times over the pump cycle. For each time, a solid line plots the energy as a function of the location of an extra charge on one of the six islands. Island numbers 0 and 7 designate the input and output electrodes. A dot indicates the minimum-energy position of the added charge as it progresses through the pump. Dashed lines show the energy when a second extra charge is introduced, with the first extra charge held on the island of minimum energy. The junction and ground capacitances are  $C_J = 0.2$  fF and  $C_g = 0.06$  fF.

island, carrying the extra charge through the pump, until it is transferred to the output electrode at  $t/\tau=7$ . As the dashed lines show, a second charge is prevented from entering the pump throughout the pump cycle.

Figure 3 was drawn assuming a bias voltage of  $V_p = -0.1$  mV between the input and output electrodes. This bias raises the energy of a charge on the output electrode 0.1 meV above the input, and requires that the pump deliver its charge to a higher-energy final state. As might be expected,

errors are more likely to occur when a charge is pumped “uphill” against a bias voltage, and such errors are the primary subject of this paper.

As in previous work,<sup>9,10</sup> we calculate the expected errors using a transition-state picture in which the probabilities  $P_n$  for occupation of the various charge states  $n$  of the pump are computed over a pump cycle. Here, the index  $n$  specifies the charge on each of the  $N-1$  islands of the pump. We will assume the charge on any given island is always  $\pm e$  or 0, so the number of possible charge states is  $3^{N-1}=729$ . In the transition-state picture, the probabilities evolve according to

$$\frac{dP_n}{dt} = \sum_{n' \neq n} (\Gamma_{nn'} P_{n'} - \Gamma_{n'n} P_n), \quad (1)$$

where  $\Gamma_{nn'}$  is the rate of transitions between states  $n'$  and  $n$ . The first term in this equation accounts for the increase in  $P_n$  due to transitions from  $n'$  to  $n$ , and the second accounts for the decrease due to transitions from  $n$  to  $n'$ . The ensemble average of the current through junction  $J$  at any instant is

$$I_J = e \sum_{n,n'} P_n [\Gamma_{n'n}^+(J) - \Gamma_{n'n}^-(J)], \quad (2)$$

where  $\Gamma_{n'n}^+(J)$  is the rate of transitions in which a charge moves in the positive direction through junction  $J$  and  $\Gamma_{n'n}^-(J)$  is the rate of transitions in which a charge moves in the negative direction through junction  $J$ . By integrating  $I_J$  over the pump cycle, we learn the total charge transferred and can determine the average counting error  $\mathcal{E}$  by comparing the result with  $e$ ,

$$\mathcal{E} = \left| \frac{1}{e} \left| \int_0^{N\tau} I_J dt \right| - 1 \right|. \quad (3)$$

Calculation of the transition rates  $\Gamma_{n'n}$  is greatly simplified for the seven-junction pump because cotunneling does not contribute significantly to counting errors and can be neglected.<sup>10</sup> Thus we consider only single-junction tunneling, but include photon-assisted processes and self-heating effects. In particular, if tunneling from island  $i$  to island  $i'$  through junction  $J$  moves the pump from state  $n$  to state  $n'$ , then the associated transition rate is<sup>10,14,22</sup>

$$\begin{aligned} \Gamma_{n'n} = & \frac{1}{e^2 R_J} \int_{-\infty}^{\infty} f_i(E) [1 - f_{i'}(E - \Delta E)] dE \\ & + \frac{\pi \alpha}{2 R_J \Delta E} \theta(\Delta E - k_B T_i), \end{aligned} \quad (4)$$

where  $\Delta E$  is the change in electrostatic energy,  $\theta$  is a unit step function, and  $f_i$  is the Fermi factor associated with island  $i$  and its electron temperature  $T_i$ :

$$f_i(E) = \frac{1}{\exp(E/k_B T_i) + 1}. \quad (5)$$

The first term in Eq. (4) accounts for thermally activated tunneling in which islands  $i$  and  $i'$  have distinct electron temperatures, while the second term accounts for photon-

assisted tunneling induced by microwave noise. The noise is assumed to have a voltage spectral density of the form  $S_V = \alpha/f$ , like that observed at low frequencies in SET electrometers.

To complete the specification of our model, we define the self-heating effect that raises the electron temperature  $T_i$  of an island above the temperature of the lattice, assumed to equal the mixing-chamber temperature  $T_{mc}$  of the dilution refrigerator used to cool the pump. Following Kautz *et al.*<sup>10,22</sup> and Niu *et al.*,<sup>15</sup> we adopt a model due to Roukes *et al.*<sup>23</sup> in which the power  $\mathcal{P}_i$  dissipated in the conduction electrons of an island is coupled to the lattice by the electron-phonon interaction. In this case, Roukes *et al.* specify that

$$T_i^5 = T_{mc}^5 + \mathcal{P}_i / (\Sigma \Omega), \quad (6)$$

where  $\Sigma$  is the electron-phonon coupling constant and  $\Omega$  is the volume of the island. To calculate the power  $\mathcal{P}_i$ , we note that tunneling from island  $i$  to  $i'$  through junction  $J$ , changing the charge state from  $n$  to  $n'$ , dissipates power  $\rho$  in both islands according to<sup>22</sup>

$$\rho_{n'n}(i) = \frac{1}{e^2 R_J} \int_{-\infty}^{\infty} (-E) f_i(E) [1 - f_{i'}(E - \Delta E)] dE, \quad (7)$$

$$\rho_{n'n}(i') = \frac{1}{e^2 R_J} \int_{-\infty}^{\infty} (E - \Delta E) f_i(E) [1 - f_{i'}(E - \Delta E)] dE. \quad (8)$$

The total power dissipated in island  $i$  due to all tunnelings averaged over the bias cycle is thus

$$\mathcal{P}_i = \frac{1}{N\tau} \sum_{n,n'} \int_0^{N\tau} \rho_{n'n}(i) P_n dt, \quad (9)$$

where the sum is understood to include all transitions  $n \rightarrow n'$  in which a charge either enters or leaves island  $i$ . Combining Eqs. (1)–(9) with the bias schedule shown in Fig. 2, we can calculate a self-consistent electron temperature  $T_i$  for each island and the counting error for the pump.

The computed counting error of a seven-junction pump with parameters similar to our experimental pump is shown in Fig. 4. For forward pumping, the error  $\mathcal{E}^+$  is large when the bias voltage is negative and the charge is being pumped uphill, as in Fig. 3. Errors in this bias region typically result because the charge escapes from the potential well and returns to the input electrode before the pump completes transfer to the output. On the other hand, a small positive bias aids forward pumping, and  $\mathcal{E}^+$  actually goes to 0 around  $V_p = 50 \mu\text{V}$ . At this voltage, errors in which the pump fails to deliver a charge are balanced by errors in which the pump delivers two charges during a bias cycle. At higher positive voltages, double charge errors become dominant and  $\mathcal{E}^+$  begins to increase again. This situation is exactly reversed for reverse pumping, with  $\mathcal{E}^-$  large for positive  $V_p$  and going to zero around  $V_p = -50 \mu\text{V}$ .

Because most experiments involve both forward and reverse pumping, it is usually advantageous to operate near  $V_p = 0$ , where both  $\mathcal{E}^+$  and  $\mathcal{E}^-$  are relatively small. For the

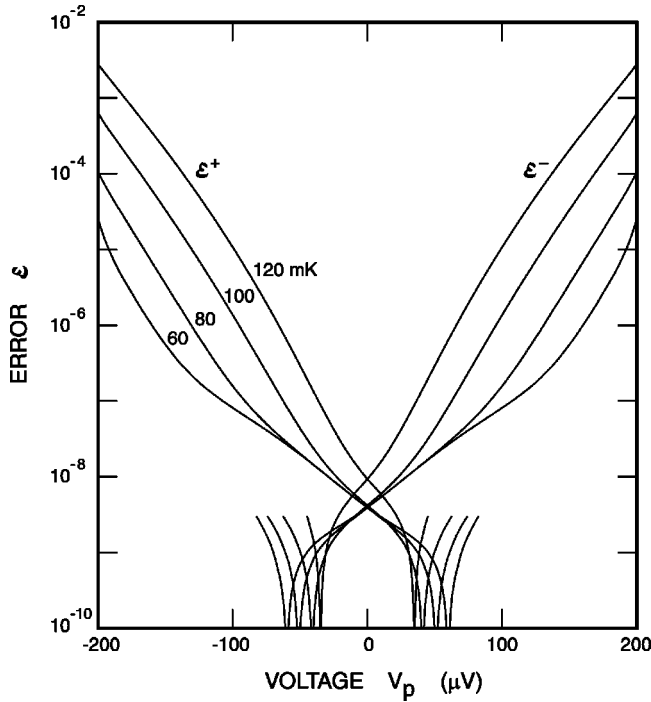


FIG. 4. Counting error as a function of bias voltage for a seven-junction electron pump with  $R_J=100$  k $\Omega$ ,  $C_J=0.2$  fF,  $C_g=0.06$  fF,  $\tau=50$  ns,  $\sqrt{\alpha}=5$  nV,  $\Sigma=0.3$  nW/K $^5$ / $\mu\text{m}^3$ , and  $\Omega=0.02$   $\mu\text{m}^3$ . Results are shown for forward and reverse pumping,  $\mathcal{E}^+$  and  $\mathcal{E}^-$ , at mixing-chamber temperatures of 60, 80, 100, and 120 mK.

cases shown in Fig. 4 with  $T_{mc} \leq 100$  mK, the errors at zero voltage are dominated by noise-induced tunneling, and the error rate is controlled by the voltage noise power  $\alpha$ . Here, we have chosen  $\sqrt{\alpha}=5$  nV, so that the total error rate,  $\mathcal{E}^+ + \mathcal{E}^-$ , is of order  $10^{-8}$ , as is typically observed experimentally in seven-junction pumps.<sup>5-7</sup> As noted elsewhere,<sup>10</sup> this level of  $1/f$  noise is consistent with that observed in SET electrometers.

In contrast to the situation at zero voltage, where the error rate is nearly independent of temperature, at voltages of 100  $\mu\text{V}$  and more, the error rate is highly sensitive to temperature. The exponential increase in errors with temperature at high voltages indicates a thermally activated process, and in this regime thermal energy provides the boost needed for a charge to escape from the pump's potential well. Details of this process are discussed in Sec. IV.

Although self-heating has been included in our simulations, it plays a relatively small role in the present case. Typical island electron temperatures, which vary only slightly with bias voltage, are roughly 71, 84, 102, and 121 mK for mixing-chamber temperatures of 60, 80, 100, and 120 mK, respectively. Thus self-heating is significant only at temperatures below about 80 mK.

### III. EXPERIMENT

Our experiment used a seven-junction electron pump fabricated by  $e$ -beam lithography using techniques described

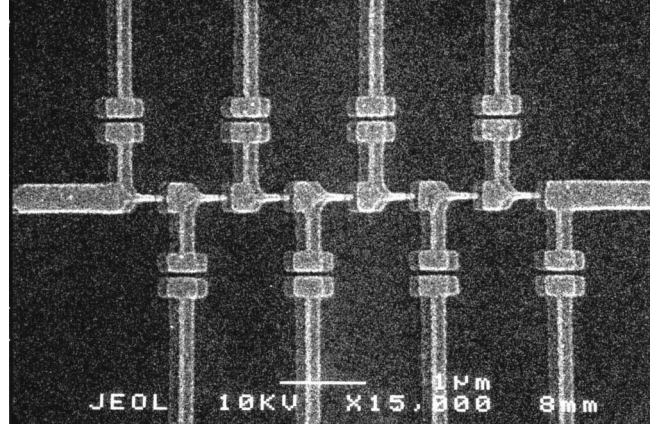


FIG. 5. Electron micrograph of an electron pump of the same design as that studied experimentally. Junctions are formed by double-angle evaporation and are located where the narrow horizontal fingers overlap the neighboring islands. Gate capacitors are formed at the gaps between opposing  $T$ 's above and below the junction array. The gate capacitors at either end of the array are not functional. The scale bar is 1  $\mu\text{m}$  in length.

elsewhere.<sup>5,6</sup> The layout of the pump is shown in Fig. 5. As in earlier devices, the circuit is aluminum deposited on a fused quartz substrate. The junctions are approximately  $6 \times 10^{-3}$   $\mu\text{m}^2$  in area. The aluminum islands have an electron-phonon coupling constant of  $\Sigma=0.3$  nW/K $^5$ / $\mu\text{m}^3$  and a volume of  $\Omega=0.018$   $\mu\text{m}^3$ .<sup>10</sup>

The pump was characterized using the capacitance-standard circuit shown in Fig. 6. Here, the capacitor to be calibrated,  $C$ , is a low-leakage cryogenic capacitor specially developed for this application.<sup>24</sup> The primary measurement tool of the circuit is an on-chip SET electrometer, consisting of gate capacitor  $C_e$  and two nanoscale tunnel junctions, which directly measures the pump voltage  $V_p$ . The circuit also includes two cryogenic needle switches, N1 and N2, that allow the circuit to be configured to perform several types of tests: measurement of the pump and electrometer parameters as well as counting errors. For example, with N1 and N2

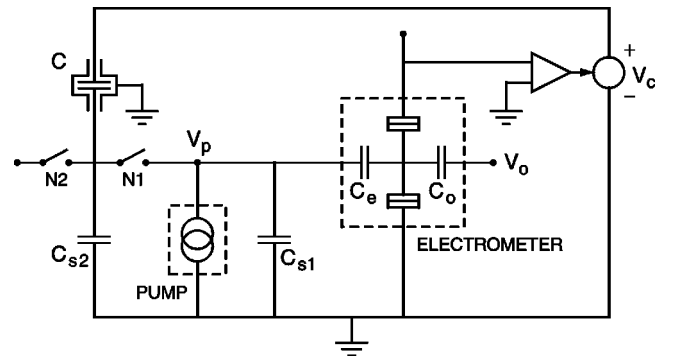


FIG. 6. Capacitance-standard and electron-pump test circuit. Here  $C \approx 2$  pF is the capacitor to be calibrated,  $C_e=0.8$  fF and  $C_o=29$  aF are gate capacitors for the electrometer,  $C_{s1} \approx 20$  fF and  $C_{s2} \approx 3$  pF are stray capacitances, and N1 and N2 are cryogenic needle switches that allow the circuit to be reconfigured while at low temperature.

closed, we measured the resistance of the pump to be  $770\text{ k}\Omega$ , indicating that the individual junctions have tunnel resistances of  $R_J = 110\text{ k}\Omega$  on average.<sup>25</sup> In addition, we subjected the pump to “electron-box,” “charge-shuttle,” and “capacitance-standard” measurements.

### A. Electron box

In order to determine the pump capacitances  $C_J$  and  $C_g$ , we performed several experiments with switch N1 open. In this configuration, the stray capacitance  $C_{s1} \approx 20\text{ fF}$  shunting the pump is relatively small, and the electrometer is sensitive enough to measure changes in  $V_p$  corresponding to charge differences that are a small fraction of  $e$ . This sensitivity allows experiments of a type first performed on an electron box by Lafarge *et al.*<sup>26</sup> and later extended to electron pumps by Keller *et al.*<sup>7</sup>

In an electron-box measurement, the pump voltage  $V_p$  is monitored while the voltage across a selected junction is varied by slowly increasing the charge bias applied to the island on one side of the junction and simultaneously decreasing the bias of the island on the other side. When a critical junction voltage is reached, tunneling becomes favorable, and the charge state of the pump changes rapidly over a small range of charge bias. This change of state is observed as a step in  $V_p$ , and the width  $2\theta_0$  of the transition, measured as a change in charge bias relative to  $e$ , is given by  $2\theta_0 = k_B T / E_c$ .<sup>7</sup> Here  $E_c = e^2 / 2(C_J + C_x)$  is the charging energy of the junction, and  $C_x$  is the total external capacitance shunting the junction. Because the pump is in thermal equilibrium during an electron-box measurement, we expect  $T$  to be the mixing-chamber temperature  $T_{mc}$ , and thus a measurement of  $2\theta_0$  can provide a direct evaluation of  $E_c$ .

Experimental values of the intrinsic transition width  $2\theta_0$  are plotted as a function of  $T_{mc}$  for junctions 1 and 5 in Fig. 7. These data display two anomalies not observed in previous pump experiments.<sup>7</sup> First, the transition width does not decrease in proportion to  $T_{mc}$  at temperatures below about 70 mK. While we are unsure of its cause, this effect was observed in the original electron-box experiments,<sup>26</sup> and may indicate that the electron temperature of the islands does not track the mixing-chamber temperature. (Because self-heating does not play a role in electron-box experiments, the heating from 60 to 71 mK estimated for pumping is not relevant here.) To calculate  $E_c$  from our data, we assume that the electron temperature equals the mixing-chamber temperature at  $T_{mc} = 80$  and 100 mK and deduce  $E_c$  from the slope of a line constrained to pass through the origin and fit these data points. The second anomaly is the distinctly different values of  $E_c$  of junctions 1 and 5, as indicated by the different slopes in Fig. 7. Charging energies for all the junctions are listed in Table I. As the table shows, the  $E_c$  for junctions 5 and 6 are significantly larger than for all other junctions, indicating that the capacitances are nonuniform and the pump is asymmetric.

In addition to the transition widths, the electron-box experiments give information about  $C_J$  and  $C_g$  through the relative amplitude of the steps in  $V_p$  produced by transitions in different junctions. Junction 1, being closest to the point

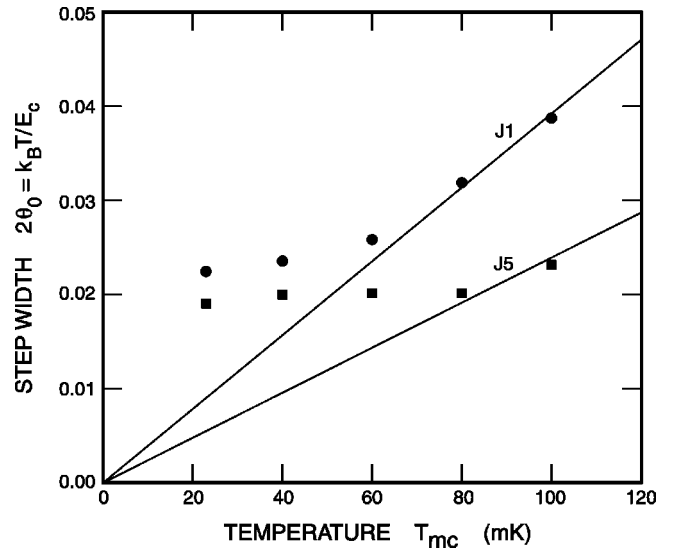


FIG. 7. Intrinsic transition width  $2\theta_0$  as a function of mixing chamber temperature  $T_{mc}$  for junctions 1 and 5, shown by circles and squares, respectively. Lines represent a least-squares fit to the data points at 80 and 100 mK, subject to the constraint that they pass through the origin.

where  $V_p$  is measured, produces the largest step, and junction 7, which is connected to this point through a long capacitance ladder, produces the smallest step. The combined information obtained from transition widths and step amplitudes allow  $C_J$  and  $C_g$  to be determined by trial-and-error adjustment. In the present case, we find a good fit to experiment assuming the capacitances listed in Table I.

In Fig. 8, we compare the experimental values of charging energy and step amplitude (filled circles) with those obtained from the ground-capacitance model using the capacitances specified in Table I (open circles). For the charging energy, we also show the result of assuming uniform junction capacitances (open squares). Although the step amplitudes predicted for junctions 2 and 3 are significantly larger than those recorded experimentally, the overall fit is satisfactory. However, assuming uniform junction capacitance clearly fails to account for the charging energies of junctions 5 and 6. As we discuss in Sec. IV, the asymmetry resulting from nonuniform  $C_J$  is important in understanding the observed error rates.

### B. Charge shuttle

The fundamental accuracy of an electron pump is most easily measured by repeatedly pumping one electron back and forth through the pump.<sup>4,5,7</sup> In our setup, this charge-shuttle experiment is performed with switch N1 open, so that single-electron errors are easily detected by the electrometer. With N1 open, the pump voltage  $V_p$  is not controlled, but it automatically adjusts itself to the point near 0 where  $\mathcal{E}^+ = \mathcal{E}^-$ . In the present case, we find that an error occurs on average about once in  $10^8$  pump cycles for  $\tau = 50\text{ ns}$ . Assuming that these errors are induced by  $1/f$  noise, we adjust the noise amplitude  $\sqrt{\alpha}$  to reproduce the observed error rate. In this way, we obtain  $\sqrt{\alpha} = 5\text{ nV}$ , a value consistent with the  $1/f$  noise observed in typical SET electrometers.<sup>10</sup>

TABLE I. Values of charging energy and junction capacitance deduced from electron-box measurements. Other pump parameters are  $C_g=0.065$  fF,  $R_J=110$  k $\Omega$ ,  $\Sigma=0.3$  nW/K $^5/\mu\text{m}^3$ ,  $\Omega=0.018$   $\mu\text{m}^3$ , and  $\sqrt{\alpha}=5$  nV.

J	1	2	3	4	5	6	7
$E_c(\text{meV})$	0.220	0.248	0.269	0.271	0.360	0.333	0.215
$C_J(\text{fF})$	0.215	0.215	0.215	0.215	0.140	0.140	0.215

With the determination of  $\alpha$ , we complete the characterization of our electron pump. All relevant parameters are listed in Table I.

### C. Capacitance standard

As its first successful application, the electron pump was used to create a standard of capacitance.<sup>8</sup> The standard is simple in concept. If a pump is used to add  $N_c$  charges to a capacitor and its voltage changes by  $\Delta V_c$ , then its capacitance is

$$C = \frac{N_c e}{\Delta V_c}. \quad (10)$$

In actual operation,<sup>8</sup> repeated trials yield a relative standard deviation of  $3 \times 10^{-7}$  for a capacitance measurement.

To measure capacitance using the circuit of Fig. 6, the needle switch N2 is opened and N1 is closed, creating a configuration first suggested by Williams *et al.*<sup>2</sup> To explain

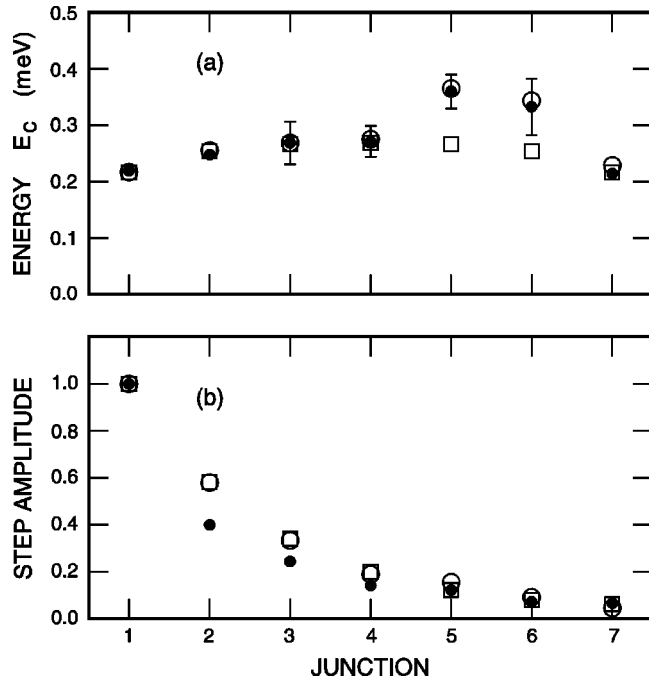


FIG. 8. Charging energy (a) and relative step amplitude (b) as a function of junction number. Filled circles show the result of electron-box measurements, open circles are calculated from the values of  $C_J$  and  $C_g$  listed in Table I, and open squares are for uniform  $C_J=0.215$  fF and  $C_g=0.065$  fF. Step amplitudes are relative to that of junction 1.

how this circuit is used to calibrate capacitor  $C$ , we first note the presence of a conducting island at potential  $V_p$  isolated by the capacitors  $C$ ,  $C_{s1}$ ,  $C_{s2}$ , and  $C_e$ . If the pump is used to transfer a known charge onto this island, the charge is generally split among the various isolating capacitors. However, if  $V_p$  is held constant, then the pumped charge is exclusively forced onto  $C$ , the capacitor under test. The task of keeping  $V_p$  fixed is accomplished by a feedback loop that uses the electrometer to monitor  $V_p$  and a controlled voltage source  $V_c$  to adjust the voltage across  $C$ . With this feedback in place,  $V_c$  changes to accommodate the pumped charge, while  $V_p$  remains constant, and the capacitance is given by Eq. (10).

As an important check of the standard's operation, charge is first pumped onto  $C$ , then the pump is reversed to confirm that  $V_c$  returns to its original value when the charge is removed. In this case, pumping errors are minimized when  $V_p \approx 0$ , since at zero bias the forward and reverse pumping errors,  $\mathcal{E}^+$  and  $\mathcal{E}^-$ , are both small. Because  $\mathcal{E}^+ + \mathcal{E}^-$  is of order  $10^{-8}$  at  $V_p=0$ , we might anticipate that capacitance calibrations can be performed with similar accuracy. However, with the pump connected to  $C$  and  $C_{s2}$ , about 5 pF in all, the change in  $V_p$  produced by a single pumped charge is much smaller than with N1 open, when all the charge goes to  $C_{s1} \approx 20$  fF. With the larger capacitance in place, the charge sensitivity of the electrometer is reduced, and the accuracy of the measurement is limited by intrinsic electrometer noise rather than pumping errors. This noise probably explains the  $3 \times 10^{-7}$  relative uncertainty of capacitance measurements made to date.<sup>8</sup>

Although the capacitance standard is normally operated with  $V_p$  near 0, the feedback circuit can also be used to hold  $V_p$  at any other value, allowing us to investigate nonideal pump operation. To set  $V_p$ , we begin with the feedback loop open, then shuttle charge back and forth until  $V_p$  settles to the point near 0 where  $\mathcal{E}^+ = \mathcal{E}^-$  and the electrometer output is constant. At this point, we close the feedback loop and apply an offset voltage  $V_o$  to the electrometer's second gate capacitor  $C_o$ . By adjusting  $V_o$ , we can change  $V_p$  according to

$$V_p = V_{p0} + \frac{C_o}{C_e} V_o, \quad (11)$$

where  $V_{p0}$  is the residual value of  $V_p$  when the feedback loop is closed. Thus it is easy to control  $V_p$  using the offset voltage  $V_o$ .

### IV. COUNTING ERRORS

After setting the feedback to maintain a given value of  $V_p$ , we can run the capacitance standard normally, as if no voltage were applied. Figure 9(a) shows a typical trace of  $V_c$  versus time when voltage-induced counting errors are significant. Here, the pump is used to repeatedly transfer  $N_c = 2^{27} = 134,217,728$  charges onto and off of capacitor  $C$ . With  $\tau = 50$  ns, about 50 s is required to complete each transfer. After a transfer is complete, the pump is maintained in its hold mode, with all charge biases set to 0, for 30 s to

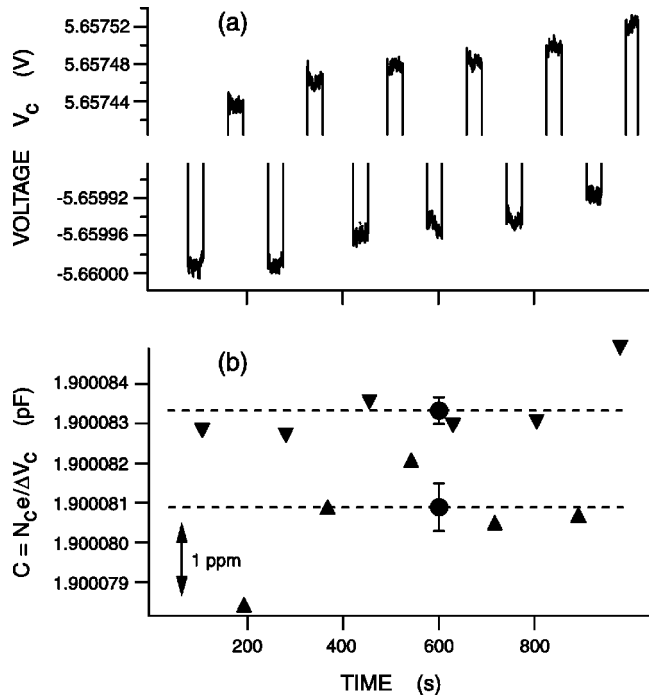


FIG. 9. (a) Feedback voltage  $V_c$  as a function of time for a capacitance calibration in which  $N_c = 2^{27} = 134,217,728$  charges are repeatedly pumped onto and then off of capacitor  $C$ . Experimental parameters are  $\tau = 50$  ns,  $T_{mc} = 37$  mK, and  $V_p \approx 100$   $\mu$ V. (b) Capacitance value deduced when pumping up (up triangles) and down (down triangles). The average capacitance values for pumping up and down are shown by filled circles and dashed lines with error bars indicating  $\pm 1\sigma$ .

allow measurement of  $V_c$ . With  $V_p \approx 100$   $\mu$ V, reverse pumping is expected to be much less accurate than forward pumping (cf. Fig. 4), and, because these errors are predominately ones in which no charge is transferred,  $V_c$  decreases by a somewhat smaller amount during reverse pumping than it increases during forward pumping. This difference accounts for the general upward trend in  $V_c$  apparent in Fig. 9(a) and provides a direct measure of the error we wish to study.

Each time the pump transfers  $N_c$  charges onto or off of capacitor  $C$ , we obtain an estimate of the capacitance from Eq. (10). The successive values of  $C$  obtained in this way are plotted in Fig. 9(b), with up triangles showing results for forward pumping and down triangles for reverse pumping. As expected from the voltage plot, capacitance estimates derived from forward and reverse pumping tend to cluster around distinctly different values. In Fig. 9(b), we show the separate averages for forward and reverse pumping as dashed lines. The difference between these averages measures the counting error, in this case associated with reverse pumping.

Experimentally determined counting errors  $\mathcal{E}$  are plotted as a function of pump voltage  $V_p$  for mixing-chamber temperatures of 40, 92, and 110 mK in Fig. 10. In this figure, we omit data points near  $V_p = 0$  where the measurements are dominated by electrometer noise rather than counting errors in the pump. How do these results compare with theory? Because all pump parameters have been determined by inde-

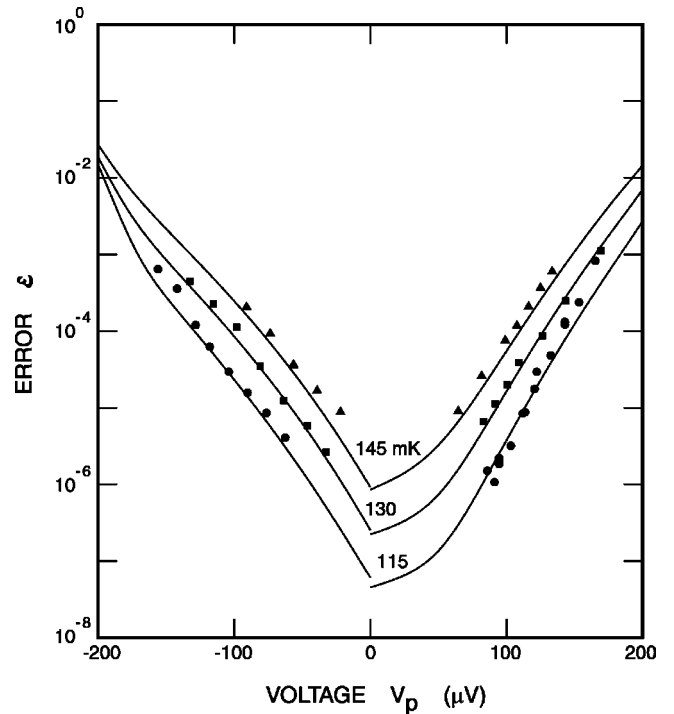


FIG. 10. Counting error  $\mathcal{E}$  as a function of pump voltage  $V_p$ . Experimental data are shown for mixing-chamber temperatures of 40 mK (circles), 92 mK (squares), and 110 mK (triangles). Solid lines show the result of simulations for temperatures of 115, 130, and 145 mK. The simulations use the parameter set listed in Table I. Because the voltage  $V_{p0}$  in Eq. (11) is not experimentally accessible, the experimental curves have been shifted in voltage to fit the simulations.

pendent measurements, we might hope to obtain an accurate fit to experiment without adjusting any parameters in the simulation. However, calculations using the experimental temperatures yield error rates significantly less than those actually observed. Thus, in Fig. 10, we show the result of simulations for temperatures of 115, 130, and 145 mK, chosen to approximately match the experimental data at 40, 92, and 110 mK, respectively. Although estimates of self-heating during pump operation indicate a base temperature for island electrons around 70 mK, we do not fully understand why a fit is obtained only if much higher temperatures are assumed. A possible explanation is that self-heating is larger than expected on the basis of the electron-phonon coupling constant  $\Sigma$  found in previous experiments.<sup>10</sup>

Although temperature was taken as an adjustable parameter, the quality of fit between theory and experiment found in Fig. 10 is excellent. In particular, the simulations reflect the same asymmetry between the errors at positive and negative voltages that is observed experimentally. The asymmetry of concern appears in Fig. 10 as a distinct difference in slope of the  $\log(\mathcal{E})$  versus  $V_p$  curves: the magnitude of the slope is between 20 and 50% larger for the positive voltage branch than the negative branch. Given the complete symmetry of Fig. 4, this asymmetry in the experimental data was at first surprising. However, an explanation was found in the fact that junctions 5 and 6 of the pump have significantly lower capacitance than the others. As Fig. 10 shows, the asymme-

try in junction capacitance completely explains the asymmetry observed in the counting errors. This agreement demonstrates that the ground-capacitance model correctly predicts the depth of the energy well that effects the transfer of charge in the pump. Overall, the agreement seen in Fig. 10 bolsters confidence in our theoretical picture of pump operation.

Using this theoretical picture, we can identify the primary error mechanism active in the pump at nonzero voltages. As it happens, the error mechanism in this case is similar to that previously identified at  $V_p = 0$ ,<sup>10</sup> but the process is thermally activated rather than driven by microwave noise. In particular, errors are most likely to occur at the point in the bias cycle, shown in Fig. 3 for  $t/\tau = 2.5$ , when the charge being pumped occupies island 2. At this point, there is a chance that thermal noise will allow the charge to surmount an energy barrier and return to the input electrode, where it remains trapped during the remainder of the bias cycle. Escape to the input can happen in either of two ways. In terms of island charges, the two error processes are

$$\text{A: } (010000) \rightarrow (100000) \rightarrow (000000),$$

$$\text{B: } (010000) \rightarrow (-110000) \rightarrow (000000),$$

where the numbers in parentheses list the charge in units of  $e$  on each of the six islands. Both of these processes transfer a charge from island 2 to the input electrode, but in A tunneling occurs first in junction 2 while in B tunneling occurs first in junction 1.

A deeper understanding of the primary error mechanism is gained from the energy diagrams corresponding to processes A and B shown in Fig. 11 for  $V_p = -0.1$  mV. At  $t/\tau = 2.25$ , the probability of the pump being in the minimum-energy  $(010000)$  state is nearly 1, and any chance of being in the  $(000000)$  state rapidly decays by tunneling to the  $(010000)$  state via  $(-110000)$ . Beginning at about  $t/\tau = 2.5$ , however, occupancy of the  $(000000)$  state can no longer decay rapidly because a barrier limits tunneling to the  $(-110000)$  state. At this time, occupation of the  $(000000)$  state begins to increase due to thermally activated tunneling from  $(010000)$  via  $(-110000)$ . The accumulation builds (open circle) until shortly after  $t/\tau = 2.5$ , when the bulk of probability (filled circle) moves on to the  $(001000)$  state. Since a small probability of being in the  $(000000)$  state remains, however, we have errors that occur by escape to the input. Because the energy of the intermediate state  $(-110000)$  is lower than that of  $(100000)$ , these errors primarily occur through process B. Thus, assuming our model applies to the experiment, process B accounts for most of the counting errors observed near  $V_p = -0.1$  mV.

As shown in Fig. 10, counting errors at high voltages,  $|V_p| > 50 \mu\text{V}$ , increase exponentially with both voltage and temperature. This observation is easily understood in terms of the energy diagram shown in Fig. 11. Because an energy barrier  $\Delta E_B$  must be overcome in the transition  $(010000) \rightarrow (-110000)$  of process B, this step limits the error rate. Assuming that all islands are at roughly the same temperature, the first term of Eq. (4) gives a rate for this limiting step proportional to the Arrhenius factor  $\exp(-\Delta E_B/k_B T)$ . That is,

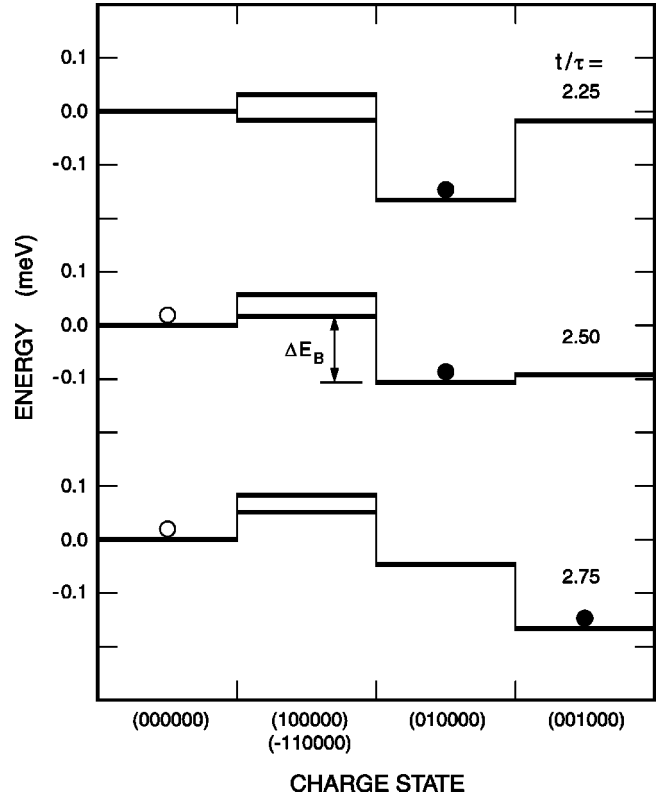


FIG. 11. Electrostatic energy as a function of charge state for selected states of a seven-junction pump with  $V_p = -0.1$  mV at three times between  $t/\tau = 2.25$  and  $2.75$ . The pump can move between adjacent states by tunneling in a single junction. Filled circles identify the state most probably occupied during normal pump operation. Open circles identify the state occupied when errors occur by thermally activated tunneling. In the second column, the higher energy level corresponds to the  $(100000)$  state and the lower one to the  $(-110000)$  state. The pump parameters are listed in Table I.

because the limiting step is thermally activated, we expect an exponential dependence on temperature and barrier energy. But  $\Delta E_B$  is linearly dependent on the pump voltage  $V_p$ , so the Arrhenius factor also translates into an exponential dependence of error on voltage. Thus we arrive at a simple qualitative explanation of the primary experimental results shown in Fig. 10.

## V. CONCLUSION

The results presented here lead to a number of conclusions regarding the application of electron pumps as capacitance standards. For the seven-junction pump under study, experiments and simulations show that, at temperatures above 100 mK and pump voltages above  $50 \mu\text{V}$ , pump errors increase exponentially with both temperature and voltage. Clearly, this high-voltage regime should be avoided in capacitance calibrations. Although calibration uncertainty at low pump voltages is presently limited to about  $3 \times 10^{-7}$  by electrometer noise, simulations and shuttle experiments suggest that uncertainties as small as  $10^{-8}$  are possible near  $V_p = 0$ , if electrometer noise can be reduced. According to

simulations in this low-voltage regime, pump voltages of a few microvolts can be tolerated without significantly affecting counting errors. Thus bias voltage is not presently an obstacle to improving the accuracy of capacitance standards.

### ACKNOWLEDGMENT

The authors are pleased to thank Neil M. Zimmerman for supplying the cryogenic capacitor used in these experiments.

\*Present address: CEA-Grenoble, DRFMC-SPSMS, 38054 Grenoble cedex 9, France.

- <sup>1</sup>H. Pothier, P. Lafarge, P.F. Orfila, C. Urbina, D. Esteve, and M.H. Devoret, *Physica B* **169**, 573 (1991); C. Urbina, H. Pothier, P. Lafarge, P.F. Orfila, D. Esteve, M. Devoret, L.J. Geerligs, V.F. Anderegg, P.A.M. Holweg, and J.E. Mooij, *IEEE Trans. Magn.* **27**, 2578 (1991); H. Pothier, P. Lafarge, C. Urbina, D. Esteve, and M.H. Devoret, *Europhys. Lett.* **17**, 249 (1992).
- <sup>2</sup>E.R. Williams, R.N. Ghosh, and J.M. Martinis, *J. Res. Natl. Inst. Stand. Technol.* **97**, 299 (1992).
- <sup>3</sup>M. W. Keller, in *Recent Advances in Metrology and Fundamental Constants*, edited by T. J. Quinn, S. Leschiutta, and P. Tavella (IOS Press, Amsterdam, 2001), p. 291.
- <sup>4</sup>J.M. Martinis, M. Nahum, and H.D. Jensen, *Phys. Rev. Lett.* **72**, 904 (1994).
- <sup>5</sup>M.W. Keller, J.M. Martinis, N.M. Zimmerman, and A.H. Steinbach, *Appl. Phys. Lett.* **69**, 1804 (1996).
- <sup>6</sup>M.W. Keller, J.M. Martinis, A.H. Steinbach, and N.M. Zimmerman, *IEEE Trans. Instrum. Meas.* **46**, 307 (1997).
- <sup>7</sup>M.W. Keller, J.M. Martinis, and R.L. Kautz, *Phys. Rev. Lett.* **80**, 4530 (1998).
- <sup>8</sup>M.W. Keller, A. Eichenberger, J.M. Martinis, and N.M. Zimmerman, *Science* **285**, 1706 (1999).
- <sup>9</sup>R.L. Kautz, M.W. Keller, and J.M. Martinis, *Phys. Rev. B* **60**, 8199 (1999).
- <sup>10</sup>R.L. Kautz, M.W. Keller, and J.M. Martinis, *Phys. Rev. B* **62**, 15 888 (2000).
- <sup>11</sup>S.V. Lotkhov, S.A. Bogoslovsky, A.B. Zorin, and J. Niemeyer, *Appl. Phys. Lett.* **78**, 946 (2001).
- <sup>12</sup>H.D. Jensen and J.M. Martinis, *Phys. Rev. B* **46**, 13 407 (1992).
- <sup>13</sup>D.V. Averin, A.A. Odintsov, and S.V. Vyshenskii, *J. Appl. Phys.* **73**, 1297 (1993).
- <sup>14</sup>J.M. Martinis and M. Nahum, *Phys. Rev. B* **48**, 18 316 (1993).
- <sup>15</sup>Q. Niu, C. Liu, H.L. Edwards, A.L. de Lozanne, and W.P. Kirk, *IEEE Trans. Instrum. Meas.* **44**, 564 (1995); C. Liu and Q. Niu, *Phys. Rep.* **286**, 349 (1997).
- <sup>16</sup>R.W. Rendell, *Phys. Rev. B* **52**, 4684 (1995).
- <sup>17</sup>L.R.C. Fonseca, A.N. Korotkov, and K.K. Likharev, *Appl. Phys. Lett.* **69**, 1858 (1996).
- <sup>18</sup>M. Covington, M.W. Keller, R.L. Kautz, and J.M. Martinis, *Phys. Rev. Lett.* **84**, 5192 (2000).
- <sup>19</sup>A.B. Zorin, S.V. Lotkhov, H. Zangerle, and J. Niemeyer, *J. Appl. Phys.* **88**, 2665 (2000).
- <sup>20</sup>A. Iwasa, A. Fukushima, and A. Sato, *Jpn. J. Appl. Phys., Part 1* **40**, 6645 (2001).
- <sup>21</sup>V. Bubanja, *J. Phys. Soc. Jpn.* **71**, 1501 (2002).
- <sup>22</sup>R.L. Kautz, G. Zimmerli, and J.M. Martinis, *J. Appl. Phys.* **73**, 2386 (1993).
- <sup>23</sup>M.L. Roukes, M.R. Freeman, R.S. Germain, R.C. Richardson, and M.B. Ketchen, *Phys. Rev. Lett.* **55**, 422 (1985).
- <sup>24</sup>N.M. Zimmerman, *IEEE Trans. Instrum. Meas.* **45**, 841 (1996).
- <sup>25</sup>The fact that the measured junction capacitances are not identical implies some variation among the tunnel resistances. However, in the absence of significant cotunneling, transition rates depend exponentially on  $C_J$  and are relatively insensitive to  $R_J$ . Thus using the average  $R_J$  is expected to be a good approximation.
- <sup>26</sup>P. Lafarge, H. Pothier, E.R. Williams, D. Esteve, C. Urbina, and M.H. Devoret, *Z. Phys. B: Condens. Matter* **85**, 327 (1991).